RESEARCH ARTICLE

Applied Polymer SCIENCE WILEY

Hybrid reinforcement of styrene-butadiene rubber nanocomposites with carbon black, silica, and graphene

Dávid Zoltán Pirityi | **Tamás Bárány** | **Kornél Pölöskei**

Department of Polymer Engineering, Faculty of Mechanical Engineering, Budapest University of Technology and Economics, Budapest, Hungary

Correspondence
Tamás Bárány, Department of Polymer Engineering, Faculty of Mechanical Engineering, Budapest University of Technology and Economics, Műegyetem rakpart 3. H-1111, Budapest, Hungary.
Email: barany@pt.bme.hu

Abstract

The complex structure of tyres makes them hard to recycle economically; hence, it is crucial to minimize the generation of tyre waste. Nano-reinforcement, such as graphene, has the potential to increase the abrasion resistance of rubber and thus their lifespan as well. In this research, hybrid styrene-butadiene rubber-based (SBR) nanocomposites reinforced with carbon black, silica and various amounts of graphene nanoplatelets are investigated with great emphasis on their combined effects on the mechanical properties of the rubber samples. Sixty-five phr of precipitated silica can holistically improve the properties of SBR. However, further addition of carbon black and graphene nanoplatelets to silica-containing samples do not benefit the properties of the samples. Further studies on the compatibilization of silica with carbon-based reinforcement are necessary. On the other hand, graphene and carbon black constitute an effective hybrid reinforcement system. The tensile strength and elongation at break of SBR are improved by almost 100% with 10 phr of graphene nanoplatelets in combination with 10 phr of carbon black. However, the abrasion resistance of samples was negatively influenced by the addition of graphene nanoplatelets whenever it was added in combination with other fillers. Silica was particularly effective in increasing the abrasion resistance of rubber.

KEYWORDS
elastomers, graphene and fullerenes, nanocomposites, rubber

1 | INTRODUCTION

The largest consumer of lightly cross-linked elastomers is the automotive tyre industry. Approximately 20 million tons of tyres are manufactured in the world each year.[1-3] Synthetic and natural rubbers constitute about half of that weight, while the rest comprises metal cords, polymer cords, fillers, lubricants, processing aids, antioxidants, and curing agents. It is important to achieve and maintain good tensile properties, tear strength, rolling resistance, wear resistance, and traction throughout the tyre's lifecycle. These properties often compromise each other and it is impossible to improve these five aspects of a product simultaneously; hence it is essential to consider various trade-offs during the material selection phase of product development. Natural rubber

(NR) is mainly used for truck tyres, while passenger car tyres are made of blends of NR and synthetic rubbers. The two most common synthetic rubbers in tyres are butadiene rubber (BR) and styrene-butadiene rubber (SBR). Their global production rates are around 3.4 and 5.3 million tons/year, respectively.[4,5]

Rubbers on their own cannot meet all criteria hence reinforcing fillers are extensively used in the rubber industry. Carbon black has been in use for over a century now. It was introduced because it significantly improved the wear resistance of rubber. Silica also became widespread filler in recent years, as the demand for high-performance, green tyres has increased. Non-polar carbon black is believed to be a more active filler because it can create better physical bonds with non-polar rubber matrices. Silica must be functionalized to promote chemical bonding with the rubber matrix. Carbon black significantly improves the hardness, wear resistance, UV resistance, tensile strength, and shear modulus of rubber while having a slight accelerator effect on curing. Meanwhile, silica can significantly decrease the rolling resistance and increase the tear strength and tensile strength of tyre rubber. Consequently, depending on the specifications, a modern tyre tread may contain 50–100 phr of silica and as little as 10 phr of carbon black in case minimal rolling resistance is required.[6–10]

Tyre recycling is challenging because they are often made of various polymer blends, consist of up to 100 various additives, and have a cross-linked structure. Currently, only downcycling options are available for rubber waste management companies. Therefore, the minimization of rubber waste generation is crucial to mitigate the environmental impact of automotive tyres. By improving the wear resistance of tyre rubber, it is possible to extend their service life; thus, fewer tyres are necessary for the same traveling distance. Consequently, the improvement of the wear resistance of tyre rubbers is a key research topic at the moment.[11–13]

Several researchers have studied the correlation between abrasion resistance and other mechanical properties. They have found that higher tensile strength, Young's modulus and Shore A hardness generally indicate higher wear resistance and thus longer tyre lifespan. Considering that these mechanical properties closely correlate with cross-link density, it can be argued that the curing system of rubbers also have a strong influence on abrasion resistance.[14–19]

Carbon black and silica have been in use for decades in the tyre manufacturing industry. Their role in achieving today's high-quality standards is irrefutable. However, a breakthrough in material properties is expected from the incorporation of novel nano reinforcement into rubbers. Several materials have been investigated: carbon nanotubes, boron nitride, cellulose nanocrystals, nanoclays, etc. One candidate that stands out is graphene. It has an exceptionally high specific surface area (2630 m^2/g) and Young's modulus (around 1 TPa). Additionally, as a carbon allotrope, it can form good adhesive bonds with organic polymers. Since its first isolation in 2004, its use in various fields has been investigated, but industrial applications are limited due to its costly manufacturing processes.[20–23]

One of the most widely studied methods for graphene production is liquid-phase exfoliation, whereby graphite is dispersed into an organic solvent and sonicated. This method yields a high-purity graphene solution of low concentration.[24] During thermal exfoliation, graphite is subjected to a thermal shock treatment, during which its layers can separate from each other. It is a well-established technology, but it cannot produce single-layer, defect-free graphene.[25] Chemical vapor deposition is also a viable process, but it is not widespread due to its costs.[24,26] Several oxidation–reduction pathways have also been developed for graphene production. The interlaminar distance of graphite oxide is two times larger than that of graphite, so the separation of layers is more facile in graphite oxide than in graphite. Hummers' method and its derivatives gained the most attention over the years. The method has high conversion rates and yields an aqueous suspension of graphene oxide, which can be reduced to form graphene.[27–31]

There are four distinct strategies for the incorporation of graphene into rubber: (a) latex mixing, (b) solution mixing, (c) in situ polymerization, and (d) melt mixing.[20,32] Latex mixing is only relevant for emulsion type synthetic rubbers or natural rubber whenever graphene is available in an aqueous dispersion (i.e. prepared by Hummers' method). This method offers the best results, as graphene agglomeration is minimized thanks to mixing graphene into rubber before drying.[33–35] Solution mixing is only relevant for solution type synthetic rubbers whenever graphene is prepared via liquid-phase exfoliation methods. Though it also offers good graphene dispersion in rubber, it has severe industrial limitations due to the additional costs of solvent regeneration. Solution mixing is mainly studied with acrylonitrile rubbers.[32,36] Most rubbers are polymerized before processing, while thermoplastic polyurethanes (TPU) are not. Consequently, in-situ polymerization can result in graphene-containing TPU nanocomposites.[37,38] During melt mixing, graphene powder is directly added to uncured rubber, similarly to other rubber additives and fillers. It is a low-cost and highly adaptable solution, as conventional mixing equipment, such as internal mixers and two-roll mills, can be used for this process. Even though this process carries the highest risk of graphene agglomeration, it can still create highly effective nano reinforcement.[25,39–41]

Song et al. compared the hybrid composites of various carbon nanofillers (carbon nanotubes, graphite and graphene) with carbon black and silica.[42] They found that 3.5 phr of graphite or carbon nanotubes do not provide significant benefits to samples with 50 phr carbon black content or 70 phr silica content. However, adding graphene would increase the samples' Young's modulus by up to 100%.

Kumar et al. investigated the melt mixing of graphene nanoplatelets into SBR-based tyre tread compounds. They compared three types of graphene nanoplatelets with a highly active carbon black grade at equal filling rates (16 phr). They found that all graphene types significantly outperformed the carbon black grade. They revealed that graphene with a high specific surface area would increase the elongation at break value of the rubber without increasing its modulus. Graphene with a lower specific surface area shifted the stress–strain curves upwards without increasing the maximum elongation significantly.[43]

Gaca et al. added 5 phr of graphene nanoplatelets to SBR and experienced a 50% increase in elongation at break and over 100% increase in tensile strength. They achieved these results via the surface modification of graphene.[44]

Malas et al. demonstrated that the mechanical properties of chloroprene rubber and chlorosulphonated polyethylene rubber were significantly enhanced by the addition of up to 9 phr of graphene oxide. They reported a 35% increase in abrasion resistance and up to 400% increase in tensile strength for their nanocomposites.[45]

Mazumder et al. prepared tyre tread compounds with large amounts of silanised silica and replaced parts of their silica content with either graphene nanoplatelets or nanoclay. The nanofillers caused an increase in the tensile strength of the samples but compromised their elongation at break. Furthermore, it was shown that both nanofillers effectively increased the abrasion resistance of rubber samples when parts of their silica contents were replaced with nanofillers.[46]

For this research, an emulsion type SBR was selected and blended with BR to imitate a real-life tyre tread composition. The hybrid reinforcement behavior of silica, carbon black and graphene nanoplatelets was investigated, whereby commercial-grade graphene was used. The high amount of silica and low amount of carbon black present in the rubber compounds follow current industrial trends in high-performance tyres. The individual effects of these three fillers in their hybrid composites have not been studied in publicly available scientific literature. Hence, the ultimate goal of this study was to reveal whether the three fillers could enhance each other's reinforcing effects. Silica and carbon black contents were fixed while graphene contents varied between 0 and 10 phr. Graphene's effects on abrasion resistance were also studied and the findings were correlated with other mechanical properties.

2 | EXPERIMENTAL

2.1 | Materials and sample preparation

Various rubber compounds, based on SBR and BR, were prepared simulating automotive tyre treads. The following ingredients were used for the mixtures:

1. SBR: SKS-30 ARKPN SBR 1502, which is an emulsion type SBR (ML_{1+4} 100°C: 52), produced by Synthez Kauchuk JSC;
2. BR: Buna CB 24, which is a solution type BR (ML_{1+4} at 100°C: 44), produced by LANXESS Deutschland GmbH;
3. Paraffin oil: DK 650 grade lubricant, produced by MOL-LUB Kft.;
4. Silica: Perkasil 408 PD, precipitated, disc-shaped silica with 20 nm average particle diameter, 170 nm agglomerate diameter (polydispersity of 2.07), and a specific surface area of 175 m^2/g, produced by Grace GmbH&Co. KG;
5. Carbon black: N330 grade amorphous, spherical carbon powder with an average particle diameter of 28–36 nm and a specific surface area of 78 m^2/g, produced by Kremenchug Carbon Black Plant;
6. Graphene nanoplatelets: xGnP Grade M with 15 μm average particle size, 6–8 nm particle thickness and a specific surface area of 120–150 m^2/g, produced by XG Sciences Inc.

Furthermore, the following ingredients were added to the compounds: zinc oxide (ZnO, produced by S.C. Werco Metal S.r.l.), stearic acid (produced by Oleon), 2,2′-dithiobisbenzothiazole (MBTS, produced by Lanxess), 1,3-diphenylguanidine (DPG, produced by Sigma-Aldrich), and sulfur (produced by Ningbo Actmix Rubber Chemicals Co., Ltd.) as curing agents and 2,2,4-trimethyl-1,1-dihydroquinoline (TMQ, produced by Kemai Chemicals Co. Ltd.) as an antioxidant.

A two-step mixing procedure was applied to rubber compounding, which is schematised in Figure 1. During the first step, four base-compounds were prepared in a Brabender Plasti-Corder internal mixer, equipped with tangential rotors. One of the compounds was unfilled, one was filled with 10 phr of carbon black, one was filled with 65 phr of silica, and one contained both carbon black and silica. Mixing took place in a chamber with a

volume of 350 cm^3 at a filling rate of 70%. Chamber temperature and rotor speed were set at 65°C and 60 rpm, respectively. Mixing was concluded when the melt temperature reached 120°C. Table 1 contains the composition of the four base-compounds.

Subsequently, graphene nanoplatelets (xGnP), antioxidants and curing agents were added to these mixtures. Four graphene contents were selected for each starting rubber mixture (0, 1, 5, and 10 phr), while all other components had the same composition in each mix. Mixing took place on a Labtech LRM-SC-110/T3E two-roll mill

(Labtech Engineering Company Ltd.) in batches of 150 g. Roll speeds and temperatures were set at 15 and 25 rpm and 50 and 70°C, respectively, and each compound was milled for 40 min. Table 2 lists the terminology for all 16 samples that only vary in their filler content.

A Collin Teach-Line Platen Press 200E (Dr. Collin GmbH) type hot press was used to cure the samples. The plates were heated up to 180°C, and the pressure was 2.8 MPa. All samples were cured for their respective t_{90} time, determined from their cure curves. Ultimately, rubber sheets with a thickness of 2 mm were obtained.
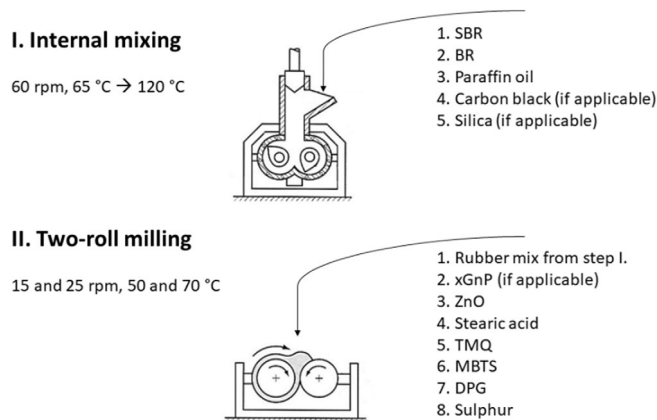
2.2 | Testing

A MonTech Monsanto D-RPA 3000 rheometer (MonTech Werkstoffprüfmaschinen GmbH,) was used to determine the curing properties of the rubber mixtures. Isothermal ($T = 180°C$) tests were ran in time sweep mode (1.667 Hz, 1° amplitude) for 10 min.

Tensile and tear strength test specimens were punched with a ball press. Tensile tests were performed on a Zwick Z005 (ZwickRoell GmbH, Ulm, Germa) tensile tester with a 5 kN load cell following ISO 37:2017 (specimen Type 1). The clamping distance was 60 mm, and the crosshead speed was 500 mm/min. The same tensile tester was used for tear strength tests with a clamping distance of 56 mm and a crosshead speed of 500 mm/

FIGURE 1 Flowchart of the two-step mixing procedure (components were added to the rubber mixture in the order shown in the scheme).

TABLE 1 Composition of the starting rubber mixtures (component contents shown in phr).

| Component | Names of the base-compounds | | | |
	Unf	CB	Si	CBSi
SBR[a]	80	80	80	80
BR[b]	20	20	20	20
Paraffin oil	30	30	30	30
Carbon black	–	10	–	10
Silica	–	–	65	65

[a]Styrene-butadiene rubber.
[b]Butadiene rubber.

TABLE 2 Nomenclature for all prepared rubber samples.

| Base-compound (Table 1) | xGnP content (phr) | | | |
	0	1	5	10
Unf	Unf0	Unf1	Unf5	Unf10
CB	CB0	CB1	CB5	CB10
Si	Si0	Si1	Si5	Si10
CBSi	CBSi0	CBSi1	CBSi5	CBSi10

Note: Each mixture contained 2.0 phr of TMQ, 3.3 phr of ZnO, 2.0 phr of stearic acid, 1.8 phr of MBTS, 1.8 phr of DPG and 1.7 phr of sulfur.

min, according to ISO 34-1:2015 (Specimen B with a 1 mm notch).

The Shore A hardness of rubber samples was determined with a Zwick H04.3150 (ZwickRoell GmbH) hardness tester. These tests were performed according to ISO 48-4:2018. The abrasive properties of rubber samples were determined on a DIN Abrasion tester (Microvision Engineering Pvt. Ltd.) according to ISO 4649:2017.

Scanning electron micrographs (SEM) were taken of the fracture surfaces of the tensile test specimens. Surfaces were first sputter-coated with gold and then placed into a Jeol JSM 6380LA (Jeol LTD.) microscope.

3 | RESULTS AND DISCUSSION

Rubber mixing took place in the tangential internal mixer. A moderate heat generation was observed for the unfilled and carbon black filled mixtures (around 30 min until 120°C). However, the temperature of the silica-containing samples reached the final temperature much faster (in around 12 min). This is due to the sheer amount of silica in the rubber compositions and its larger specific surface area. Another important observation during mixing was that oil had to be added in small batches;

otherwise, it would cause slippage between the rotors and the rubber, thus reducing the shearing effects. After mixing, the curing properties of each mixture were determined. The resulting curing curves are shown in Figures 2 and 3. For samples without silica, it is visible that the larger the graphene content, the larger the maximum torque values, indicating some reinforcement. Interestingly, the addition of 10 phr of carbon black decreased the maximum torque of the samples. Another important trend is that graphene caused the samples to go through vulcanization reversion sooner and to a greater extent, which can be compensated with large amounts of fillers.

In Figure 3, it is visible that the silica content changed the vulcanization curves significantly. They shifted upwards, indicating a strong reinforcing effect. In addition, silica decreased the curing rate of the samples while keeping the scorch time intact. Thus, it significantly increased the t_{90} values of the samples. This phenomenon can be attributed to silica's basic pH. In addition, when silica was present in the mixture, the addition of graphene reduced the maximum torque values, which contradicts the trend for the samples without silica, indicating incompatibility between silica and graphene.

Tensile tests were performed on each sample, and the resulting stress–strain curves are presented in Figures 4
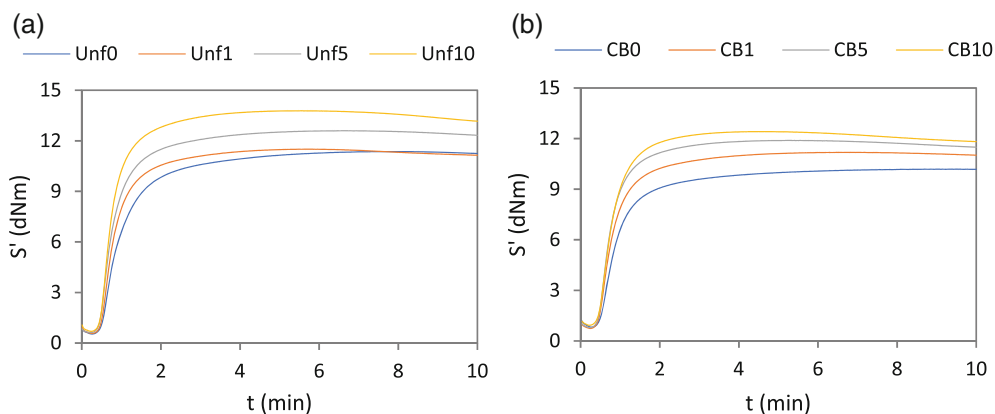

FIGURE 2 Curing curves for the unfilled (a) and carbon black filled (b) experimental sets. [Color figure can be viewed at wileyonlinelibrary.com]
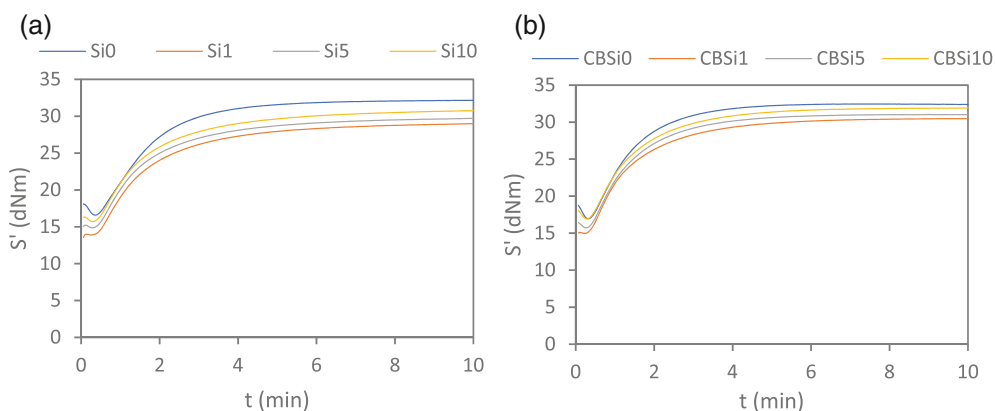

FIGURE 3 Curing curves for the silica-filled (a) and silica and carbon black filled (b) experimental sets. [Color figure can be viewed at wileyonlinelibrary.com]

and 5. The addition of graphene to the otherwise unfilled samples had beneficial effects on the tensile properties. The curves of Unf0 and Unf1 overlap until the unfilled sample's failure, indicating equal Young's moduli. However, 1 phr of xGnP increased the tensile strength and the elongation at break values of the sample by around 20%. A further increase in xGnP content shifted the curves upwards, signifying an increase in modulus as well. This phenomenon can be explained by surpassing the percolation threshold of graphene and thus, the upwards shift shows that xGnP acts more like a traditional reinforcement at 5 and 10 phr content.

When 10 phr of carbon black was added to the system, similar trends were observed. The tensile properties of Unf0 and CB0 are almost identical (with CB0 having a slightly larger Young's modulus and tensile strength). The curves belonging to CB0 and CB1 coincide until CB0's failure, similarly to Unf0 and Unf1. At 5 and 10 phr xGnP contents, the curves shifted upwards as well. However, this phenomenon was coupled with an additional increase in elongation at break values. Ultimately, the CB5 and CB10 significantly outperform what could be estimated based on the results of Unf0, Unf5, Unf10 and CB0. Consequently, it can be stated that carbon black and xGnP comprise an effective hybrid reinforcing system. Similar trends have been reported by other research groups, and the increase in elongation at break at larger filling rates indicates a good stress transfer between nanoparticles and the matrix.[47,48]

The addition of 65 phr of silica significantly improved the tensile properties of the samples. However, additional xGnP increased the modulus only, while the elongation at break of the samples was severely compromised. Furthermore, the combined use of silica, carbon black and graphene decreased the otherwise outstanding elongation at break even further. These phenomena indicate that the three fillers weaken each other's reinforcing capabilities.

In Figure 6, the tensile strength and elongation at break values were plotted against xGnP content for the samples containing no silica. These graphs further showcase the steady increase in these properties at increasing xGnP contents, proving the effectiveness of the xGnP-CB hybrid reinforcement system.

The tear strength of the rubber samples was also measured, which is a crucial property for tyre rubbers as crack propagation resistance is related to these values. The numerical results are summarized in Table 3, together with other measured properties. Graphene content seems to have an irregular impact on the tear strength of rubber compounds, though the trends are similar to those observed for tensile properties. For the 'Unf' and 'CB' experimental sets, graphene significantly improved the tear strength of the samples. The combination of carbon black and graphene was especially effective. When silica
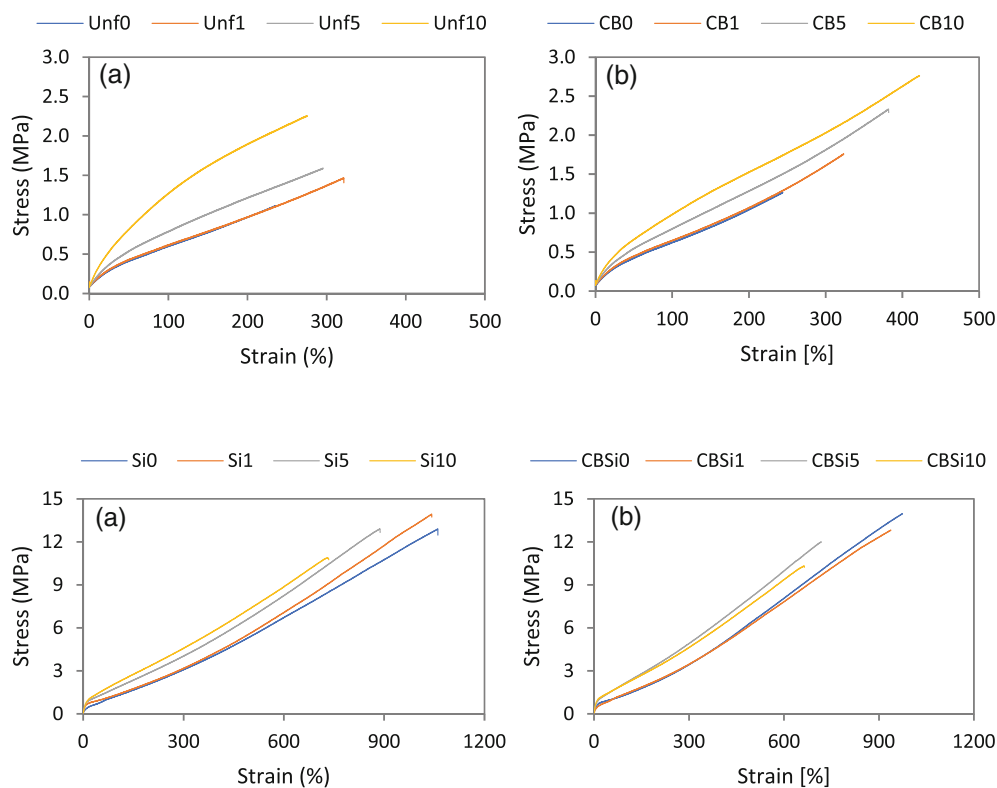

FIGURE 4 Stress–strain curves for the unfilled (a) and carbon black filled (b) experimental sets. [Color figure can be viewed at wileyonlinelibrary.com]

FIGURE 5 Stress–strain curves for the silica-filled (a), and silica and carbon black filled (b) experimental sets. [Color figure can be viewed at wileyonlinelibrary.com]

FIGURE 6 Tensile test results versus xGnP content: tensile strength (a) and elongation at break (b). [Color figure can be viewed at wileyonlinelibrary.com]
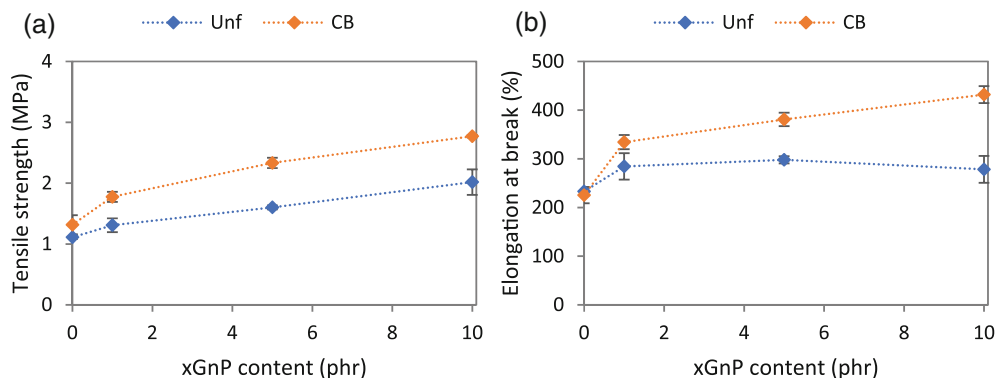

TABLE 3 Summary of tensile and tear strength test results.

| Sample	S'_{min} (dNm)	S'_{max} (dNm)	$t_{0.1}$ (s)	$t_{0.9}$ (s)	Tensile strength (MPa)	Elongation at break (%)	Tear strength (N mm^{-1})	Abrasion loss (mm^3)
Unf0	0.54	11.36	33	148	1.11 ± 0.03	233 ± 8	3.26 ± 0.05	214 ± 23
Unf1	0.57	11.50	32	112	1.31 ± 0.11	284 ± 27	3.54 ± 0.24	200 ± 24
Unf5	0.62	12.60	30	115	1.60 ± 0.03	298 ± 7	5.34 ± 0.27	182 ± 3
Unf10	0.70	13.78	30	103	2.02 ± 0.21	278 ± 28	4.38 ± 0.53	203 ± 22
CB0	0.82	10.19	32	132	1.32 ± 0.16	226 ± 17	5.51 ± 0.94	123 ± 13
CB1	0.74	11.18	30	106	1.78 ± 0.08	334 ± 15	5.48 ± 0.39	113 ± 20
CB5	0.79	11.89	29	98	2.33 ± 0.09	381 ± 14	6.86 ± 0.37	158 ± 7
CB10	0.93	12.42	30	95	2.77 ± 0.02	432 ± 17	8.48 ± 0.49	168 ± 2
Si0	16.59	32.16	39	252	12.61 ± 1.23	1067 ± 8	33.11 ± 1.74	55 ± 2
Si1	11.86	29.00	N/A	238	13.37 ± 0.79	1064 ± 31	32.05 ± 1.96	61 ± 3
Si5	13.51	29.71	24	239	12.11 ± 0.73	890 ± 42	34.14 ± 0.18	66 ± 4
Si10	14.67	30.75	28	251	10.88 ± 0.66	764 ± 71	29.82 ± 0.92	96 ± 6
CBSi0	16.95	32.46	34	180	13.30 ± 0.95	944 ± 43	41.27 ± 3.58	54 ± 3
CBSi1	14.30	30.48	26	208	12.54 ± 0.29	889 ± 78	44.07 ± 12.62	61 ± 1
CBSi5	15.73	31.03	31	195	12.61 ± 0.73	752 ± 42	35.70 ± 6.41	80 ± 3
CBSi10	16.92	31.91	32	208	10.71 ± 0.34	656 ± 43	32.23 ± 1.45	96 ± 3
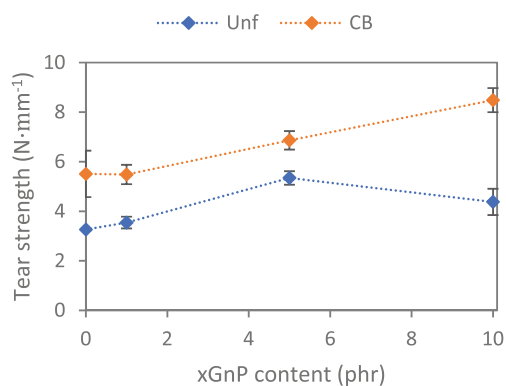
FIGURE 7 Tear strength versus xGnP content for samples without silica. [Color figure can be viewed at wileyonlinelibrary.com]

was introduced to the system, the property greatly improved, yet graphene provided no additional benefit, except for sample CBSi1. However, the standard deviation in the experimental data of CBSi1 is much higher than that of other samples, making this improvement doubtful. Also, the addition of carbon black to the samples with silica improved the tear strength in all cases, indicating that larger carbon particle effectively improve this property, probably because cracks can only propagate around the particles rather than by breaking them in half.

Figure 7 further demonstrates the effectiveness of the xGnP-CB hybrid system for the samples containing no silica. A quasi-linear increase in tear strength is observed for the 'CB' experimental set, while for the 'Unf' sample set, there is a slight decrease above 5 phr.

Figure 8a shows the Shore A hardness of the rubber samples. These results show a clear trend: the more additives present in the rubber compounds, the harder they

are. In Figure 8b, the abrasion loss of all samples is plotted against their xGnP content. It is shown that xGnP increased the abrasion loss of the samples in three out of
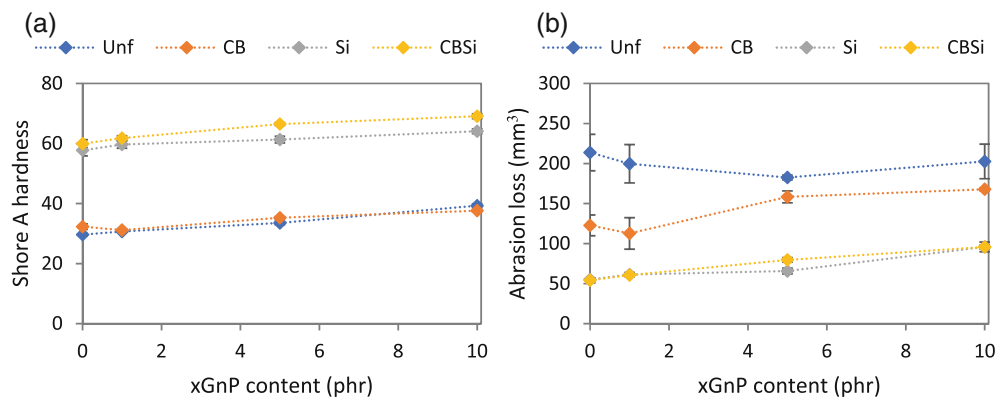

FIGURE 8 (a) Shore A hardness versus xGnP content and (b) abrasion loss versus xGnP content. [Color figure can be viewed at wileyonlinelibrary.com]

TABLE 4 ANOVA results for rubber samples with no silica.

	Source of variation	SS	df	MS	F	p value	F_{crit}
Tensile strength	Between groups	6.994	7	0.999	81.52	7.870×10^{-12}	2.614
	Within groups	0.208	17	0.0123			
	Total	7.202	24				
Elongation at break	Between groups	1.065×10^5	7	15209.2	43.50	1.253×10^{-9}	2.614
	Within groups	5943	17	349.6			
	Total	1.124×10^5	24				
Tear strength	Between groups	62.14	7	8.877	39.03	6.872×10^{-9}	2.657
	Within groups	3.639	16	0.2275			
	Total	65.78	23				
Abrasion loss	Between groups	3.469×10^{-2}	7	4.956×10^{-3}	15.53	1.899×10^{-12}	2.577
	Within groups	5.743×10^{-3}	18	3.191×10^{-4}			
	Total	4.043×10^{-2}	25				

TABLE 5 ANOVA results for rubber samples with silica.

	Source of variation	SS	df	MS	F	p value	F_{crit}
Tensile strength	Between groups	18.43	7	2.633	4.635	7.146×10^{-3}	2.764
	Within groups	7.955	14	0.5682			
	Total	26.39	21				
Elongation at break	Between groups	4.175×10^5	7	59,639	23.21	1.119×10^{-6}	2.764
	Within groups	35,978	14	2570			
	Total	4.534×10^5	21				
Tear strength	Between groups	506.6	7	72.38	2.597	5.398×10^{-2}	2.657
	Within groups	445.9	16	27.87			
	Total	952.5	23				
Abrasion loss	Between groups	1.472×10^{-2}	7	2.103×10^{-3}	105.4	3.483×10^{-12}	2.657
	Within groups	3.191×10^{-4}	16	1.994×10^{-5}			
	Total	1.504×10^{-2}	23				

TABLE 6 Tukey–Kramer results for rubber samples without silica.

Sample pair	Tensile strength			Elongation at break			Tear strength			Abrasion loss		
	$|x_i - x_j|$	T	T/F	$|x_i - x_j|$	T	T/F	$|x_i - x_j|$	T	T/F	$|x_i - x_j|$	T	T/F
Unf0–Unf1	0.198	0.291	FALSE	51	49	TRUE	0.279	1.348	FALSE	0.011	0.050	**FALSE**
Unf0–Unf5	0.491	0.311	TRUE	65	52	TRUE	2.080	1.348	TRUE	0.018	0.056	**FALSE**
Unf0–Unf10	0.907	0.311	TRUE	45	52	FALSE	1.113	1.348	FALSE	0.013	0.047	**FALSE**
Unf0–CB0	0.207	0.311	FALSE	8	52	FALSE	2.243	1.348	TRUE	0.075	0.047	TRUE
Unf0–CB1	0.665	0.311	TRUE	101	52	TRUE	2.218	1.348	TRUE	0.084	0.044	TRUE
Unf0–CB5	1.222	0.311	TRUE	148	52	TRUE	3.599	1.348	TRUE	0.031	0.050	FALSE
Unf0–CB10	**1.661**	**0.311**	**TRUE**	**199**	**52**	**TRUE**	**5.220**	**1.348**	**TRUE**	0.013	0.056	FALSE
Unf1–Unf5	0.293	0.291	TRUE	14	49	FALSE	1.801	1.348	TRUE	0.007	0.056	FALSE
Unf1–Unf10	0.709	0.291	TRUE	6	49	FALSE	0.835	1.348	FALSE	0.024	0.047	FALSE
Unf1–CB0	0.008	0.291	FALSE	59	49	TRUE	1.964	1.348	TRUE	0.065	0.047	TRUE
Unf1–CB1	0.467	0.291	TRUE	50	49	TRUE	1.939	1.348	TRUE	0.074	0.044	TRUE
Unf1–CB5	1.024	0.291	TRUE	96	49	TRUE	3.320	1.348	TRUE	0.020	0.050	FALSE
Unf1–CB10	1.462	0.291	TRUE	147	49	TRUE	4.941	1.348	TRUE	0.002	0.056	FALSE
Unf5–Unf10	0.416	0.311	TRUE	20	52	FALSE	0.966	1.348	FALSE	0.031	0.053	FALSE
Unf5–CB0	0.285	0.311	FALSE	72	52	TRUE	0.163	1.348	FALSE	0.057	0.053	TRUE
Unf5–CB1	0.174	0.311	FALSE	36	52	FALSE	0.138	1.348	FALSE	0.066	0.051	TRUE
Unf5–CB5	0.731	0.311	TRUE	83	52	TRUE	1.520	1.348	TRUE	0.013	0.056	FALSE
Unf5–CB10	1.169	0.311	TRUE	134	52	TRUE	3.140	1.348	TRUE	0.005	0.061	FALSE
Unf10–CB0	0.700	0.311	TRUE	53	52	TRUE	1.129	1.348	FALSE	0.088	0.043	TRUE
Unf10–CB1	0.242	0.311	FALSE	56	52	TRUE	1.105	1.348	FALSE	0.097	0.041	TRUE
Unf10–CB5	0.315	0.311	TRUE	103	52	TRUE	2.486	1.348	TRUE	0.044	0.047	FALSE
Unf10–CB10	0.754	0.311	TRUE	154	52	TRUE	4.106	1.348	TRUE	0.026	0.053	FALSE
CB0–CB1	0.458	0.311	**TRUE**	109	52	**TRUE**	0.024	1.348	FALSE	0.009	0.041	FALSE
CB0–CB5	1.015	0.311	**TRUE**	155	52	**TRUE**	1.357	1.348	**TRUE**	0.044	0.047	FALSE
CB0–CB10	**1.454**	**0.311**	**TRUE**	**206**	**52**	**TRUE**	**2.977**	**1.348**	**TRUE**	**0.062**	**0.053**	**TRUE**
CB1–CB5	0.557	0.311	**TRUE**	47	52	FALSE	1.381	1.348	**TRUE**	0.053	0.044	TRUE
CB1–CB10	0.996	0.311	**TRUE**	98	52	**TRUE**	3.001	1.348	**TRUE**	0.071	0.051	TRUE
CB5–CB10	0.439	0.311	**TRUE**	51	52	FALSE	1.620	1.348	**TRUE**	0.018	0.056	FALSE

Note: Values that showcase the trends mentioned in the text are highlighted in bold.

four experimental runs. This contradicts the expectations of graphene's capabilities of increasing wear resistance. However, similar trends are also observed in the literature, indicating that graphene's precursor graphite is sometimes applied as a lubricant in certain operations.[49,50] When the effects of xGnP are disregarded, a clear reverse correlation between abrasion loss and Shore A hardness is observed. Silica is widely renowned for its beneficial effects on rubbers' wear properties, so it is not surprising that the 'Si' and 'CBSi' experimental runs significantly outperformed the ones without silica. It should be noted that due to the low tear strength and hardness of 'Unf' and 'CB' experimental runs, abrasion was dominated by matrix disintegration, involving lots of smearing. On the other hand, silica-containing samples showed proper abrasion phenomena.

To further demonstrate how tensile strength, elongation at break, tear strength and abrasion loss depend on the silica, carbon black and xGnP content of the samples, a statistical analysis has been performed on these mechanical properties. Analysis of variance (ANOVA) and Tukey–Kramer test were selected to show whether there are significant differences between properties of certain samples. In all cases, samples containing silica and those without silica were treated separately, as silica always caused at least a 50% change in the values. ANOVA results for samples without silica are presented in Table 4. In the table's header, SS stands for the sum of

squares, df stands for degrees of freedom, MS stands for mean squares, F is the ratio between the mean square between the groups and the average square within the groups, p value is the significance probability parameter, and F_{crit} is a tabulated parameter corresponding to a 0.05 confidence interval. In Table 4, each F value is larger than its corresponding F_{crit} value, indicating that the null hypothesis of each sample having the same average values can be rejected. Consequently, the Tukey–Kramer test shall be performed on each pair of samples to determine which samples have significantly different mechanical properties. In Table 5, the analogous ANOVA results for silica-containing samples are presented. In this case, F is larger than F_{crit} for three

properties, indicating that the null hypothesis is only accepted for tear strength. Consequently, it can be concluded that when 65 phr of silica is added to the system, neither 10 phr of xGnP nor 10 phr of carbon black has a significant effect on the tear strength of rubber compounds. Tukey–Kramer tests can be performed for the other three properties.

Tukey–Kramer test results for samples not containing silica are summarized in Table 6. In the header, $|x_i - x_j|$ stands for the pairwise difference between the means, T stands for the Tukey–Kramer minimal honest significance, and T/F stands for true or false, whereby true means a significant difference between the means (if $|x_i - x_j| > T$). The most noteworthy parts of Table 6

TABLE 7 Tukey–Kramer results for rubber samples without silica.

Sample pair	Tensile strength			Elongation at break			Abrasion loss		
	$|x_i - x_j|$	T	T/F	$|x_i - x_j|$	T	T/F	$|x_i - x_j|$	T	T/F
Si0–Si1	0.77	2.43	**FALSE**	3	163	**FALSE**	0.009	0.013	**FALSE**
Si0–Si5	0.50	2.17	**FALSE**	177	146	**TRUE**	0.016	0.013	**TRUE**
Si0–Si10	1.73	2.17	**FALSE**	302	146	**TRUE**	0.060	0.013	**TRUE**
Si0–CBSi0	**0.69**	**2.43**	**FALSE**	**123**	**163**	**FALSE**	**0.004**	**0.013**	**FALSE**
Si0–CBSi1	0.07	2.17	**FALSE**	177	146	TRUE	0.013	0.013	TRUE
Si0–CBSi5	0.00	2.17	**FALSE**	315	146	TRUE	0.042	0.013	TRUE
Si0–CBSi10	1.90	2.17	**FALSE**	411	146	TRUE	0.068	0.013	TRUE
Si1–Si5	1.26	2.43	**FALSE**	174	163	TRUE	0.008	0.013	FALSE
Si1–Si10	2.49	2.43	**TRUE**	300	163	TRUE	0.052	0.013	TRUE
Si1–CBSi0	0.08	2.66	**FALSE**	120	179	FALSE	0.005	0.013	FALSE
Si1–CBSi1	0.83	2.43	**FALSE**	175	163	TRUE	0.005	0.013	FALSE
Si1–CBSi5	0.77	2.43	**FALSE**	312	163	TRUE	0.034	0.013	TRUE
Si1–CBSi10	2.67	2.43	**TRUE**	408	163	TRUE	0.059	0.013	TRUE
Si5–Si10	1.23	2.17	**FALSE**	126	146	FALSE	0.044	0.013	TRUE
Si5–CBSi0	1.19	2.43	**FALSE**	54	163	FALSE	0.012	0.013	FALSE
Si5–CBSi1	0.43	2.17	**FALSE**	1	146	FALSE	0.003	0.013	FALSE
Si5–CBSi5	0.50	2.17	**FALSE**	138	146	FALSE	0.026	0.013	TRUE
Si5–CBSi10	1.41	2.17	**FALSE**	234	146	TRUE	0.052	0.013	TRUE
Si10–CBSi0	2.41	2.43	**FALSE**	180	163	TRUE	0.056	0.013	TRUE
Si10–CBSi1	1.66	2.17	**FALSE**	125	146	FALSE	0.047	0.013	TRUE
Si10–CBSi5	1.73	2.17	**FALSE**	12	146	FALSE	0.018	0.013	TRUE
Si10–CBSi10	0.18	2.17	**FALSE**	109	146	FALSE	0.008	0.013	FALSE
CBSi0–CBSi1	0.75	2.43	**FALSE**	55	163	**FALSE**	0.010	0.013	**FALSE**
CBSi0–CBSi5	0.69	2.43	**FALSE**	192	163	**TRUE**	0.038	0.013	**TRUE**
CBSi0–CBSi10	2.59	2.43	**TRUE**	288	163	**TRUE**	0.064	0.013	**TRUE**
CBSi1–CBSi5	0.07	2.17	**FALSE**	137	146	FALSE	0.029	0.013	TRUE
CBSi1–CBSi10	1.84	2.17	**FALSE**	233	146	TRUE	0.055	0.013	TRUE
CBSi5–CBSi10	1.90	2.17	**FALSE**	96	146	FALSE	0.026	0.013	TRUE

Note: Values that showcase the trends mentioned in the text are highlighted in bold.

are highlighted in bold. Abrasion loss was not significantly affected by the addition of xGnP to otherwise unfilled samples. Even incremental amounts of xGnP caused a significant increase in tensile strength, and elongation at break and tear strength for samples with CB.

An analogous Tukey–Kramer test was performed for the silica-containing samples as well (Table 7). For tensile strength, most values are false, indicating no dependence of tensile strength on the various amounts of CB or xGnP. For the elongation at break and abrasion loss values, a statistically significant deterioration can be observed when increasing the xGnP content from 0 to 5 or 10 phr. Overall, the predominance of TRUE values in Table 6, compared to the predominance of FALSE values in
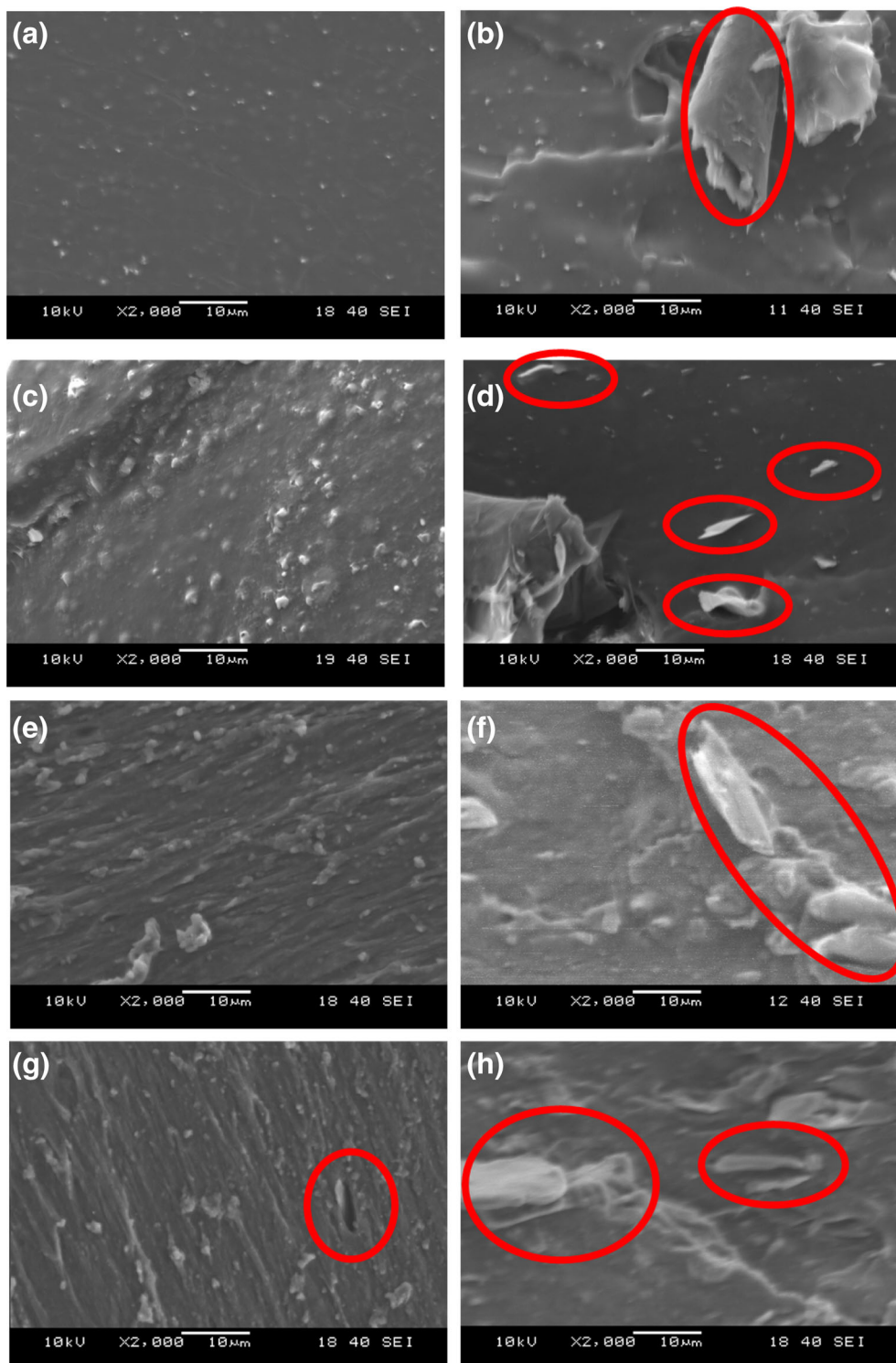
FIGURE 9 Scanning electron microscopy micrographs of the fracture surfaces of the rubber samples: (a) Unf0, (b) Unf5, (c) CB0, (d) CB5, (e) Si0, (f) Si5, (g) CBSi0, and (h) CBSi5 [Color figure can be viewed at wileyonlinelibrary.com]

Table 7 suggests that xGnP and CB have a relatively larger influence on material properties when no silica is present in the system.

Scanning electron micrographs of the fracture surfaces of selected samples are shown in Figure 9. The morphology of the samples was studied to understand how the various hybrid reinforcement compositions impacted the mechanical properties of the samples.

Figure 9a shows the smooth surface of the completely unfilled Unf0 sample. In Figure 9b, xGnP's characteristic layered structure can be identified. This particular particle, visible in the top right corner of the micrograph, did not contribute to the reinforcement as it was perpendicular to the load. In Figure 9d, the thin white stripes also show the presence of xGnP, but this time they are parallel to the load, indicating stronger reinforcing capabilities. The mechanical properties of the samples also support these claims. The orientation of xGnP particles heavily depends on their adhesion to the rubber matrix. Carbon black enhanced the adhesion of xGnP to the rubber matrix, allowing it to take higher loads. In Figure 9c, no such phenomenon can be observed for sample CB0, as the fracture surface runs along the surfaces of individual carbon black particles.

The introduction of silica significantly changed the fracture surface. Individual silica particles are easily identified in Figure 9e, homogeneously distributed across the surface. The addition of graphene and carbon black to this mixture disrupted this balance by creating voids and irregularities in the sample, as shown in Figure 9f–h. The previously explained thin strips are not visible in silica-reinforced samples, indicating that graphene did not take significant loads.

4 | CONCLUSION

In this work, four sets of SBR-based composites were prepared, differing from each other in their filler compositions: only (a) did not contain either carbon black or silica, (b) contained 10 phr of carbon black, (c) contained 65 phr of silica, and (d) contained 10 phr of carbon black and 65 phr of silica. Each set consisted of four samples containing various amounts of graphene nanoplatelets (0, 1, 5, or 10 phr).

Cure tests showed that carbon black and xGnP accelerated the cross-linking reactions while silica slowed them. Mechanical and morphological tests revealed several trends concerning the effects of the filler materials. Each of the fillers provided detectable reinforcement to SBR when introduced to the rubber on its own. However, their combinations were not always effective. Rubber compounds with 65 phr of silica significantly outperformed those containing only graphene and carbon black. However, silica was incompatible with both carbon-based fillers. Adding carbon black and graphene to silica-containing rubber samples significantly decreased their elongation at break values.

When combined, carbon black and graphene have synergistic effects on the properties of rubber compounds. When both are present in a rubber composite, it has better mechanical properties than those anticipated based on the individual impacts of carbon black and xGnP. These trends are supported by morphology studies that showed that carbon black aided the homogeneous dispersion of xGnP, allowing it to take larger loads.

Abrasion tests showed that wear resistance corresponds well with rubber hardness. In addition, silica significantly improved the abrasion resistance of the rubber samples, while graphene nanoplatelets had an adverse impact. Overall, it was shown that 10 phr of carbon black and up to 10 phr of graphene nanoplatelets could not impact the mechanical properties of rubber samples with 65 phr of silica as much as in the case of silica-less samples. Furthermore, when silica is used in the system, it should be surface-treated to increase its compatibility with carbon black and graphene nanoplatelets.

ORCID
Dávid Zoltán Pirityi https://orcid.org/0000-0003-2574-8077
Tamás Bárány https://orcid.org/0000-0002-9196-7852
Kornél Pölöskei https://orcid.org/0000-0001-7439-2949

PIRITYI ET AL.

REFERENCES

[1] Beroe, Styrene Butadiene Rubber (SBR) Commodity Report. Accessed 11 January, 2022. https://www.beroeinc.com/commodity/sbr-market/, **2019**.

[2] P. Europe, Plastics—the Facts 2019; an analysis of European plastics production, demand and waste data. Accessed 11 January, 2022. https://plasticseurope.org/wp-content/uploads/2021/10/2019-Plastics-the-facts.pdf, **2019**.

[3] Iinternational Rubber Study Group, Rubber Statistical Bulletin, April–June 2017. Accessed 11 January, 2022. https://www.rubberstudy.org/reports, **2017**.

[4] C. K. Varnava, C. S. Patrickios, *Polymer* **2021**, *215*, 123322.

[5] I. Z. Halász, D. Kocsis, D. Á. Simon, A. Kohári, T. Bárány, *Period. Polytech. Chem. Eng.* **2020**, *64*, 248.

[6] A. Afzal, A. Kausar, M. Siddiq, *Polym.-Plast. Technol. Eng.* **2017**, *56*, 573.

[7] X. Wang, L. Wu, H. Yu, T. Xiao, H. Li, J. Yang, *E-Polymers* **2021**, *21*, 279.

[8] R. J. Dhanorkar, S. Mohanty, V. K. Gupta, *Ind. Eng. Chem. Res.* **2021**, *60*, 4517.

[9] G. J. Papakonstantopoulos, B. Jiang and B. R. Hahn, EP2990218B1, **2015**.

[10] M. Jarnthong, Z. Peng, N. Lopattananon, C. Nakason, *Express Polym. Lett.* **2021**, *15*, 1135.

[11] M. Forrest, in *Overview of the World Rubber Recycling Market*, Vol. 1 (Ed: D. Potter), Smithers Rapra, Shawbury **2014**, p. 17.

[12] A. I. Isayev, in *Recycling of Rubbers*, Vol. 1 (Eds: J. E. Mark, B. Erman, C. M. Roland), Elsevier, Amsterdam **2013**, p. 697.

[13] The European Parliament and the Council of the European Union: Directive 2008/98/EC of the European Parliament and of the Council of 19 November 2008 on waste and repealing certain Directives, OJ L 312, 22.11. **2008**.

[14] K. Pal, S. K. Pal, C. K. Das, J. K. Kim, in *Elastomeric Nanocomposites for Tyre Applications* (Eds: V. Mittal, J. K. Kim, K. Pal), Springer, Berlin, Heidelberg **2011**, p. 201.

[15] B. N. J. Persson, *J. Chem. Phys.* **2001**, *115*, 3840.

[16] N. Rattanasom, T. Saowapark, C. Deeprasertkul, *Polym. Test.* **2007**, *26*, 369.

[17] C. Hong, H. Kim, C. Ryu, C. Nah, Y.-I. Huh, S. Kaang, *J. Mater. Sci.* **2007**, *42*, 8391.

[18] K. Pal, R. Rajasekar, D. J. Kang, Z. X. Zhang, S. K. Pal, C. K. Das, J. K. Kim, *Mater. Des.* **2010**, *31*, 677.

[19] G. Milani, F. Milani, *J. Appl. Polym. Sci.* **2021**, *138*, 50073.

[20] A. Pazat, C. Barres, F. Bruno, C. Janin, E. Beyou, *Polym. Rev.* **2018**, *58*, 403.

[21] V. Gopalan, P. Bhardwaj, N. Satonkar, V. Pragasam, *Mech. Eng.* **2020**, *64*, 248.

[22] A. Ahamad, P. Kumar, *Compos. Commun.* **2020**, *22*, 100440.

[23] L. Cao, Z. Gong, C. Xu, Y. Chen, A. C. S. Sustain, *Chem. Eng.* **2021**, *9*, 9409.

[24] D. G. Papageorgiou, I. A. Konloch, R. J. Young, *Carbon* **2015**, *95*, 460.

[25] J. R. Potts, O. Shankar, S. Murali, L. Du, R. S. Ruoff, *Compos. Sci. Technol.* **2013**, *74*, 166.

[26] C. R. Herron, K. S. Coleman, R. S. Edwards, B. G. Mendis, *J. Mater. Chem.* **2011**, *21*, 3378.

[27] W. S. Hummers, R. E. Offeman, *J. Am. Chem. Soc.* **1958**, *80*, 1339.

[28] R. Alibeyli, A. Ata, E. Topaç, *ISITES* **2014**, *2014*, 1.

[29] D. C. Marcano, D. V. Kosynkin, J. M. Berlin, A. Sinitskii, Z. Sun, A. Slesarev, L. B. Alemany, W. Lu, J. M. Tour, *ACS Nano.* **2010**, *4*, 4806.

[30] S. Schopp, R. Thomann, K.-F. Ratzsch, S. Kerling, V. Altstädt, R. Mülhaupt, *Macromol. Mater. Eng.* **2013**, *299*, 319.

[31] V. Acar, S. Erden, M. Sarikanat, Y. Seki, H. Akbulut, M. O. Seydibeyoglu, *Express Polym. Lett.* **2020**, *14*, 1106.

[32] E. George, J. Joy, S. Anas, *Polym. Compos.* **2021**, *42*, 4961.

[33] Y. Zhan, J. Wu, H. Xia, N. Yan, G. Fei, G. Yuan, *Macromol. Mater. Eng.* **2011**, *296*, 590.

[34] L. Sorrentino, M. Aurilia, in *Graphite- and Graphene Based Nanocomposites*, Vol. II (Ed: K. D. Sattler), CRC Press, Boca Raton **2016**, p. 675.

[35] G. C. Psarras, in *Nanographite-Polymer Composites*, Vol. II (Ed: K. D. Sattler), CRC Press, Boca Raton **2016**, p. 647.

[36] B. Mensah, D. Kumar, D.-K. Lim, S. G. Kim, B.-H. Jeong, C. Nah, *J. Appl. Polym. Sci.* **2015**, *132*, 42457.

[37] H. Kim, Y. Miura, C. W. Macosko, *Chem. Mater.* **2010**, *22*, 3441.

[38] B. Mensah, K. C. Gupta, H. Kim, W. Wang, K.-U. Jeong, C. Nah, *Polym. Test.* **2018**, *68*, 160.

[39] H. Guo, P. Ji, I. Z. Halász, D. Z. Pirityi, T. Bárány, Z. Xu, L. Zheng, L. Zhang, L. Liu, S. Wen, *Materials* **2020**, *13*, 5746.

[40] Z. Tang, L. Zhang, W. Feng, B. Guo, F. Liu, D. Jia, *Macromolecules* **2014**, *47*, 8663.

[41] P. Berki, K. László, N. T. Tung, J. Karger-Kocsis, *J. Reinf. Plast. Compos.* **2017**, *36*, 808.

[42] S.-H. Song, O.-S. Kwon, H.-K. Jeong, Y.-G. Kang, *Korean J. Mater. Res.* **2010**, *20*, 104.

[43] V. Kumar, T. Hanel, L. Giannini, M. Galimberti, U. Giese, *Kaut. Gummi Kunst.* **2014**, *67*, 29.

[44] M. Gaca, C. Vaulot, M. Maciejewska, M. Lipińska, *Materials* **2020**, *13*, 5407.

[45] A. Malas, C. K. Das, *Compos. Part B* **2015**, *79*, 639.

[46] A. Mazumder, J. Chanda, S. Bhattacharyya, S. Dasgupta, R. Mukhopadhyay, A. K. Bhowmick, *J. Appl. Polym. Sci.* **2021**, *138*, 51236.

[47] S. Mondal, D. Khastgir, *Compos. Part A* **2017**, *102*, 154.

[48] T. Gspann, N. Montinaro, A. Pantano, J. Elliott, A. Windle, *Carbon* **2015**, *93*, 1021.

[49] Y. Fan, Q. Li, X. Li, D. H. Lee, U. R. Cho, *Carbon Lett* **2018**, *27*, 72.

[50] L. L. Wang, L. Q. Zhang, M. Tian, *Mater. Des.* **2012**, *39*, 450.